Available online at www.sciencedirect.com
ScienceDirect
Wear 264 (2008) 211–218
WEAR
www.elsevier.com/locate/wear

Erosion model on alumina ceramics: A retrospection, validation and refinement

K.R. Gopi [a,*], R. Nagarajan [a], S.S. Rao [b], S. Mandal [b]

[a] *Department of Chemical Engineering, IIT Madras, Chennai 600036, India*
[b] *Ceramics Division, Carborundum Universal Ltd., Hosur 635126, India*

Received 9 May 2006; received in revised form 28 January 2007; accepted 8 March 2007
Available online 17 April 2007

Abstract

Erosion due to coal particles has a detrimental effect on economy of power plants. Alumina ceramic-lined pipelines and cyclones are in common use for fluid-laden coal transportation and separation. Several brittle erosion models are available for air-jet and slurry jet erosion in literature. From these, the most-cited erosion models were identified. An orthogonal fractional–factorial experimental matrix which includes all possible variables that contribute to brittle erosion was designed, conducted and validated. This paper gives a comparison between the most-cited literature model and a model developed on the basics of our experimental data. In general, slurry erosion models obtained experimentally were found to have better agreement with literature models when compared to air-jet erosion models. The reason for deviation of experimentally derived models from literature models is systematically studied and rationalized.

Keywords: Brittle materials; Erosion model; Air-jet erosion; Slurry erosion; Elastic modulus

1. Introduction

Pulverized coals from bowl mills are transported to boilers through pipelines lined with wear resistant alumina ceramics. Structural ceramics like alumina in the form of tiles are used as lining material in pipelines to reduce wear losses. Alumina ceramics are predominantly used for this purpose because of low cost, high hardness, good corrosion resistance and high wear resistance compared to metals. Coal transportation and associated erosion are complex phenomena. Erosion is a function of a number of parameters like coal particle velocity, angle of impingement, diameter and density of the particle, hardness of both particle and target materials, fracture toughness of the target materials and concentration of slurry.

Typical erosion models emphasize that erosion rate is a function of target material properties like fracture toughness, hardness and target material density. When striking particles are assumed as non-deforming, the applicability of the model cited in Ref. [1] is limited to soft targets. Other models cited [2–7] take into account both particle and target properties as factors affecting erosion rate. Models cited in Ref. [2] are valid for gas/particle high concentration erosion. The authors have here included target density as an additional parameter. In the models cited in Ref. [8], erosion rate of alumina ceramic is related to velocity and size of four different particles at normal-incidence. The authors predicted that velocity exponent increases with decreasing hardness and toughness of erodent. In the model cited in Ref. [9], volume loss of substrate is related to parameters like particle velocity, mass of abrasive particles, angle of impingement, fraction of particles cut in an idealized manner and plastic flow pressure.

Some models [10–12] include the angle of impingement as an additional parameter, represented in trigonometric terms. Angle of impingement of particle on target is one of the key factors in determining erosion rate. In Ref. [11], the authors have included threshold velocity and threshold particle size terms. The model cited in Ref. [12] holds good for slurry erosion with high concentration. This model predicts that erosion rate increases as the angle of impingement increases, and shows a decreasing trend with increasing particle flux. This model predicts that fine grain alumina with inter-granular glassy phase is the right candidate material which offers high erosive wear resistance, but the

* Corresponding author. Tel.: +91 44 22574158; fax: +91 44 22574152.
E-mail addresses: krgopi@iitm.ac.in, kr_gopi@yahoo.com (K.R. Gopi).

0043-1648/$ – see front matter © 2007 Elsevier B.V. All rights reserved.
doi:10.1016/j.wear.2007.03.002

Nomenclature

C_L	crack length (μm)
d_p	diameter of particle (g/cm^3)
DOE	design of experiment
E, E_R	erosion rate (g)
f	particle volume fraction
g	grams
H, T_H	hardness of target (kg/mm^2)
HLA	high level analyses
K_{ct}	fracture toughness of target (MPa $\sqrt{m}$)
l	liter
lpm	liter per minute.
P_H	hardness of particle (kg/mm^2)
Q	volumetric flow rate of slurry
v	slurry velocity (m/s)
V_p	velocity of the particle (m/s)

Greek symbols

α	angle of impingement of particles (°)
ρ_p	density of particle (g/cm^3)
ρ_t	density of target (g/cm^3)

authors have not included the microstructure as a parameter in their wear model. Structural ceramics with fine grain size [12] were found to have more erosive wear resistance than coarse grains, i.e., erosive wear increases with grain size. The model cited in Ref. [13] shows high dependence of erosion on shape characteristics of a pit due to impact of particle on target.

2. Proposed erosion models for brittle materials

2.1. Gas/particle "low" concentration [5,12]

$$E \propto V_p^{2.8} d_p^{0.66} \rho_p^{1.3} K_{ct}^{-1.33} H^{-0.25} \sin^2\alpha$$

2.2. Gas/particle "high" concentration [1,5,12]

$$E \propto V_p^{2.8} d_p^{0.66} \rho_p^{1.3} \rho_t K_{ct}^{-1.33} H^{-0.25} \sin^2\alpha$$

2.3. Slurry/particle "high" concentration [12]

$$E \propto (v\rho_p f)^{-.0.3551} (\sin\ \alpha)^{1.623}$$

The above-mentioned models have been formulated by reviewing the most-cited models in published literature. Models 2.1 and 2.2 without trigonometric term are most accepted models for dry-impact erosion; the trigonometric term has been added since alumina ceramic tiles find application in pipeline bends and cyclone separators, which are angular at several impact locations. Models 2.1 and 2.2 were formulated from Refs. [1,5,12]. Model 2.3 was obtained from Ref. [12]. In case of slurry erosion, fewer models are available in literature. The power law exponent for $\sin\alpha$ in model 2.3 was obtained from the experimental data points of Ref. [12]. In general, value of exponents for erosion parameters in above proposed models were obtained by two ways: by averaging the value of power law exponents found in most-cited literature models, or by taking directly the value of exponents found in the most-cited literature model, as appropriate.

Table 1
Particle used for experiment

Materials	Density (g/cm^3)	Vickers hardness (kg/mm^2)
Coal (particle)	1.6	1620–1655
Alumina (particle)	3.99	2130–2150
Silicon carbide (particle)	3.21	2430–2470

3. Experimental program

3.1. Materials

Three different materials, alumina, SiC and coal, were selected as erodents and three different types of alumina tile were selected as target material. The choice of materials was based on factors like commercial availability, widespread application and acceleration characteristics. The properties of erodent materials are given in Table 1. Hardness of coal was calculated approximately from cumulative hardness of inorganic matters present in the coal.

3.2. Experimental procedure

An L 27 orthogonal fractional–factorial design of experiment (DOE) was defined to develop a comprehensive in-house model by investigating the effects of six parameters, at three levels. Two replicates were run under each condition to improve statistical validity. Target substrates were subjected to analyses for properties such as elastic modulus, shear modulus, fracture toughness, hardness and surface roughness. Vickers's hardness [14] and fracture toughness [15] were measured by conventional diamond indentation method. Elastic modulus, shear modulus, Poisson's ratio are measured with the help of sound velocity by ultrasonic pulse-echo technique [16].

3.2.1. Air-jet erosion tester

Sandblast-type erosion test rig shown in Fig. 1 was used to carry out air borne erosion tests. The erodent particles were entrained in a stream of compressed air and accelerated down a 65 mm long nozzle with 5 mm internal diameter to impact on a target mounted on an angle fixture (30°, 45° and 90°). The particle velocity can be measured using the rotating double disk technique [17] and it can be adjusted to desired values by using compressed air pressure.

Air borne erosion tests were carried out for three types of alumina target. The dimensions of the specimen were 30 mm × 30 mm × 5 mm. The target samples were polished in order to have a smooth surface finish. The initial weight of the target was taken in an analytical balance of ±0.01 mg accuracy. The target specimens were mounted 10 mm from nozzle orifice for all impingement angles. Each sample was eroded with a fixed amount of erodent at velocities of 20, 30 and 40 m/s. The test

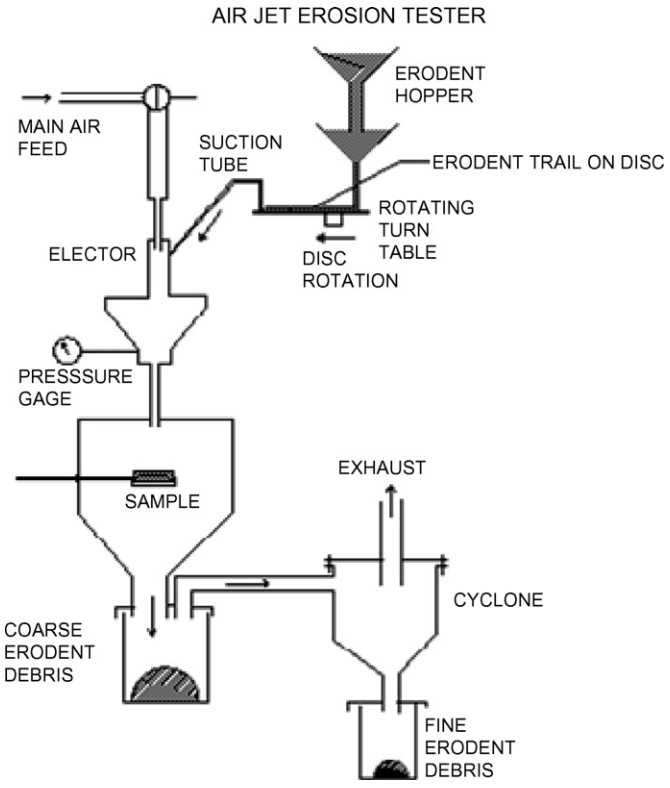

Fig. 1. Air-jet erosion tester.

duration was 5 min. At the end of each test, the target sample was taken out, cleaned, dried and weighed to calculate mass loss. This mass loss is taken to represent erosion loss.

3.2.2. Slurry-impact erosion tester

A simple slurry pot tester shown in Fig. 2 was used to carry out slurry erosion test. A slurry of specified concentration was prepared by mixing an appropriate quantity of erodent particles with water and introducing into the slurry pot. The typical parts of slurry tester are a slurry holding tank, an agitator, a diaphragm pump, air compressor, an ejector nozzle and a sample holder. The slurry, a mixture of potable water and erodent particle, was pumped from holding tank to ejector nozzle of inner diameter 6.1 mm.

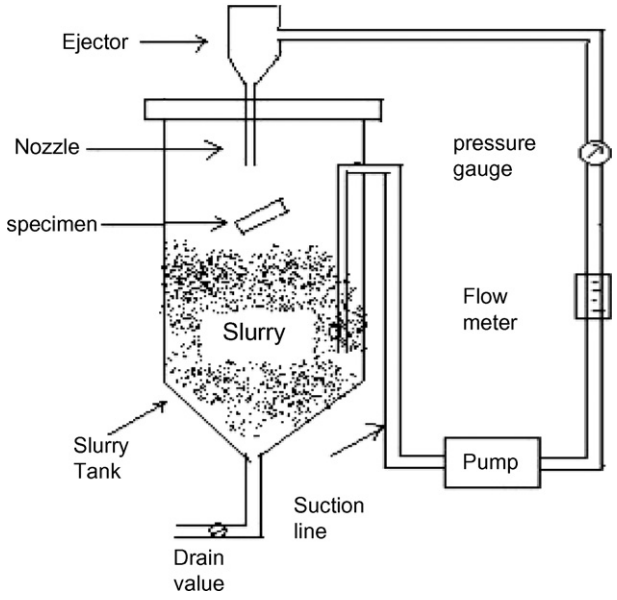

Fig. 2. Slurry-impact erosion tester.

It emerges as a high velocity jet to impact the target surface. Velocity of slurry jet was controlled by adjusting the compressed air pressure. The angle of impingement was varied by tilting the target sample holder through a mechanical lever. The major variables examined were: velocity of impinging slurry, angle of impingement, hardness, diameter and density of particle, density and fracture toughness of target. The test duration was 30 min. The target specimen was initially weighed in an analytical balance of 0.01 mg accuracy. At the end of the each test, the specimen was taken out, cleaned, dried and weighed. This mass loss was taken to represent erosion loss (Tables 2–4).

4. Experimental results and data analysis

Experimental data are presented in Figs. 3–12.

High level analysis (HLA) is performed by averaging measured data for each level of a single parameter, then plotting the averaged data against all the levels of that parameter. The results obtained from the above data analyses are compiled as comprehensive model displayed in Tables 5 and 6. Two paral-

Table 2
Air-jet erosion experimental matrix

Level	Particle velocity (m/s)	Angle of impingement (°)	Particle diameter (micrometer)	Particle type	Feed rate (g/min)	Target
1	20	30	63–75	SiC	2	Alumina-A
2	30	45	105–120	Alumina	3	Alumina-B
3	40	90	120–150	Coal	4	Alumina-C

Table 3
Slurry jet erosion experimental matrix

Level	Particle flow rate (lpm)	Angle of impingement (°)	Particle diameter (μm)	Particle type	Particle concentration (g/l)	Target
1	15	30	63–75	SiC	10	Alumina-A
2	17.5	60	105–120	Alumina	15	Alumina-B
3	20	90	120–150	Coal	20	Alumina-C

Table 4
Mechanical properties of target materials

Target properties	Alumina-A	Alumina-B	Alumina-C
Vickers hardness (kg/mm^2)	1215–1245	1200–1240	1320–1370
Crack length (μm)	41.8	45.3	48.5
Density (g/cm^3)	3.58	3.59	3.67
Young's modulus (GPa)	239	217	299
Shear modulus (GPa)	98.2	89.4	121.1
Poisson ratio	0.217	0.215	0.237
Fracture toughness (MPa $\sqrt{m}$)	5.16	4.41	4.43
Surface roughness, R_a (μm)	0.885	0.802	0.826
Maximum roughness depth, R_{max} (μm)	12.9	23.8	13.9

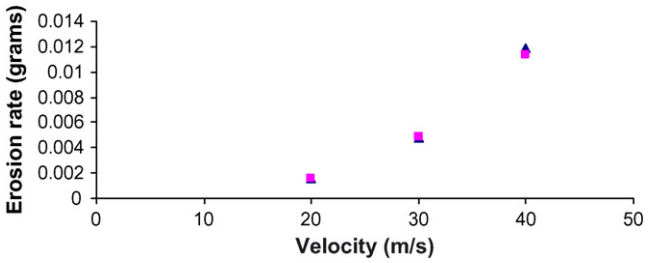

Fig. 3. Erosion rate as a function of particle velocity (HLA) dry-impact.

lel experiments with each set of parameters were performed; the data points are shown in Figs. 3–8, which give the range of parameters. HLA has high statistical significance, since a large number of data points are available for analyses. In our experiment, the 18 erosion data points measured (9 for each level of each parameter) can be conveniently analyzed in this manner.

Fig. 3 shows that erosion rate increases with increase in particle velocity for dry-impact erosion. A power law exponent which varies from 2.82 to 2.92 is obtained for velocity of particle, which is in the same range as in the most-cited literature model. The range of the velocity exponents varies from 1.5 to 3.2 in literature models. Erosion increases with sine of the angle of impact, with exponent ranging from 2.31 to 2.35 for dry-impact and 1.45 to 1.48 for slurry-impact as shown in Fig. 4(a) and (b), respectively; these are in line with literature models.

Erosion increases with particle size up to about 100 μm for both dry-impact and slurry-impact, as shown in Figs. 5(a) and (b), respectively. A polynomial relationship is obtained in case of dry-impact, whereas a power law relationship, with exponent value ranging from 0.77 to 0.9, is obtained in case of slurry-impact. In this case, there is a good agreement with most-cited literature erosion model in case of slurry-impact. For dry-impact, hardness has significant erosion effect only above 20 GPa as shown in Fig. 6(a). Erosion increases as particle hardness to the power ranging from 3.35 to 3.6 for slurry-impact as shown in Fig. 6(b). The range of hardness exponent varies from −0.25 to 2.3 in literature. Erosion has a maximum for particle density around 3 g/cm^3 for both dry-impact and slurry-impact, as shown in Fig. 7(a) and (b), respectively. The range of particle density

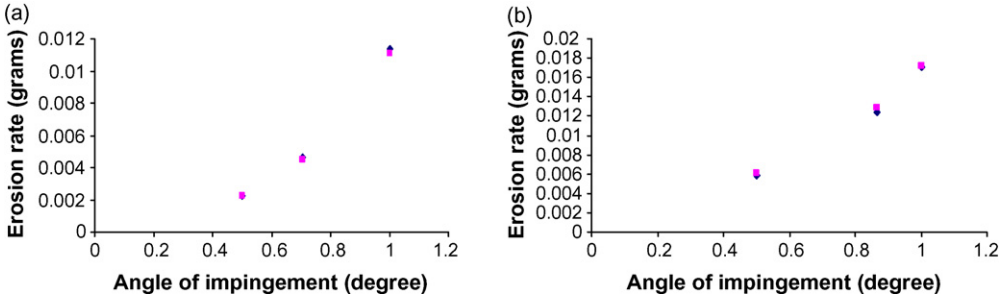

Fig. 4. (a) Erosion rate as a function of angle of impingement (HLA) dry-impact. (b) Erosion rate as a function of angle of impingement (HLA) slurry-impact.

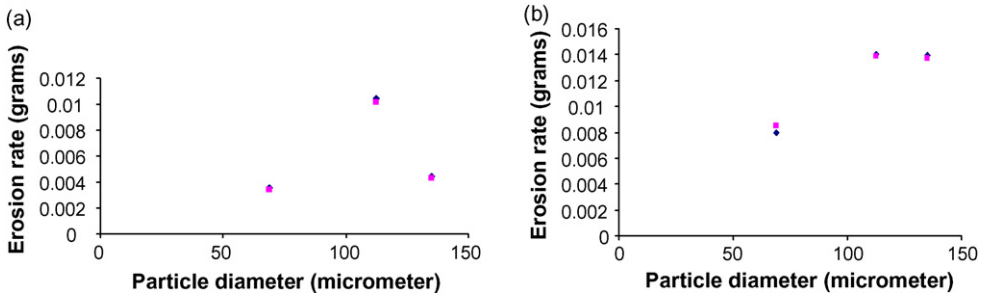

Fig. 5. (a) Erosion rate as a function of particle diameter (HLA) dry-impact. (b) Erosion rate as a function of particle diameter (HLA) slurry-impact.

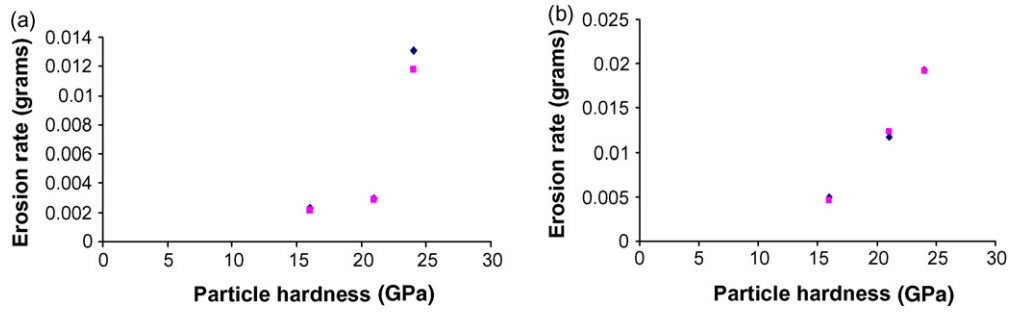

Fig. 6. (a) Erosion rate as a function of particle hardness (HLA) dry-impact. (b) Erosion rate as a function of particle hardness (HLA) slurry-impact.

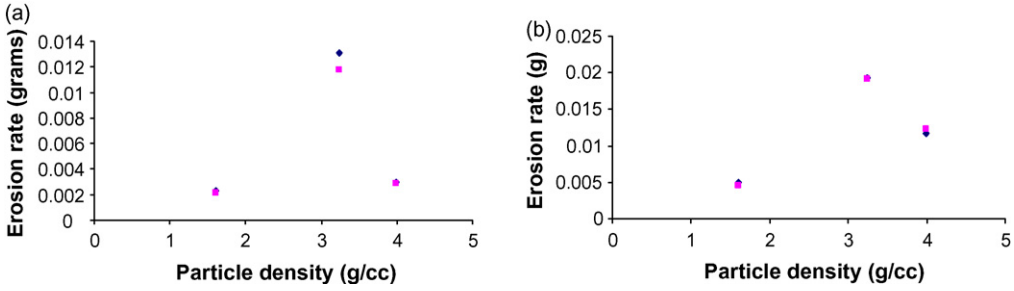

Fig. 7. (a) Erosion rate as a function of particle density (HLA) dry-impact. (b) Erosion rate as a function of particle density (HLA) slurry-impact.

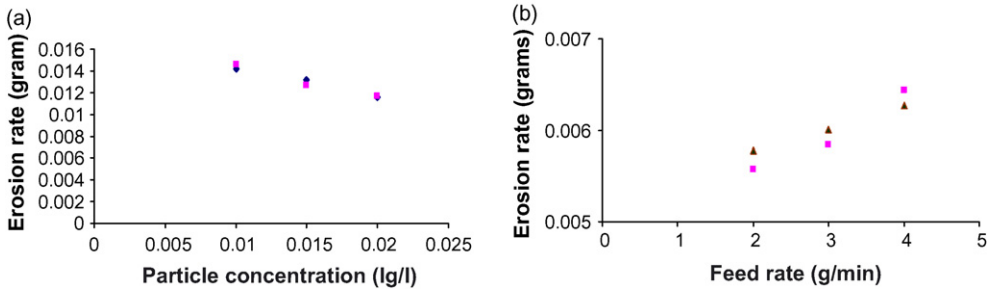

Fig. 8. (a) Erosion rate as a function of particle concentration (HLA) slurry-impact. (b) Erosion rate as a function of particle feed rate (HLA) dry-impact.

exponent varies from 0.25 to 1.3 in literature, whereas a polynomial relationship is obtained in our case. Erosion decreases with particle concentration as shown in Fig. 8(a), to the power ranging from −0.28 to −0.32, which exactly matches the literature value. Erosion increases slightly with feed rate in dry-impaction as shown in Fig. 8(b).

5. Target properties versus erosion rate

Comparison was made by non-dimensionalizing target properties and erosion rates at 30° and 90° angle of impingement with respect to target properties and erosion rates of Alumina-A ceramic. Fig. 9(a) and (b) represents the above-mentioned com-

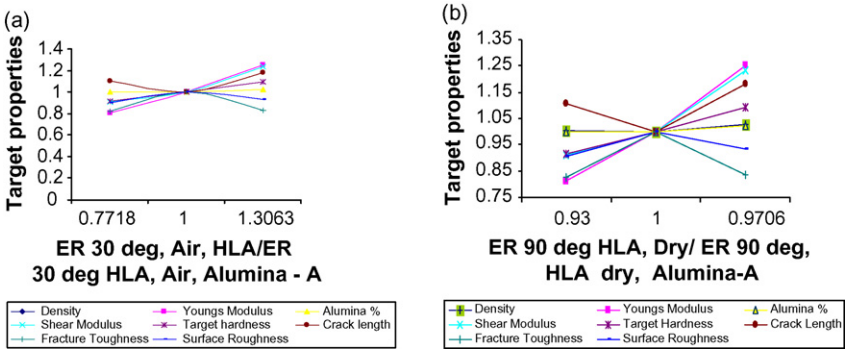

Fig. 9. (a) Comparison of target properties with erosion rate measured at 30° impingement for dry-impact. (b) Comparison of target properties with erosion rate measured at 90° for dry-impact.

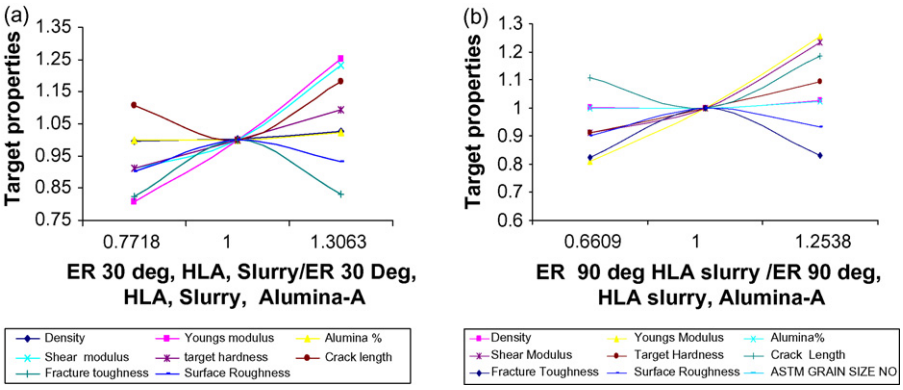

Fig. 10. (a) Comparison of target properties with erosion rate measured at 30° impingement for slurry-impact. (b) Comparison of target properties with erosion rate measured at 90° for slurry-impact.

parison for dry-impact erosion at 30° impact and 90° impact. Fig. 10(a) and (b) represents the same comparison for slurry erosion at 30° impacts and 90° impacts. Elastic modulus of target material appears to be a key variable in low-angle impact erosion and in normal-incidence for both dry-impact and slurry erosion. Erosion rate increases with increase in elastic modulus. In Ref. [18], it is stated that a brittle material with a high elastic modulus can fail catastrophically, unable to withstand accidental overloading during service. Brittle materials with high elastic moduli are not considered suitable as structural members [18].

6. Second-order effects

In second-order effect analyses, the effect of erosion parameters on erosion rates of individual ceramic targets like Alumina-A, Alumina-B, and Alumina-C were studied. Results of second-order effect analysis compare very well with high level analyses, which suggests that our test procedures were acceptably consistent, and that all tested ceramics show similar erosion characteristics.

For example, velocity exponent range for Alumina-A, Alumina-B and Alumina-C ceramics are 2.8–3.13, 3.3–3.6 and 2.3–2.5 as shown in Fig. 11(a)–(c), respectively, and the angle of impingement exponent is 2.1–2.5, 2.64–2.7 and 1.9–2.3 as shown in Fig. 12(a)–(c), respectively.

7. Summary

Based on dry-impact and slurry erosion tests conducted, the following parametric-dependences have been determined, and compared with models from literature (Tables 5 and 6).

In general, our experimental data corroborate literature models. Where there are differences, we conclude that our efficient design of experiment (DOE) has enabled incorporation of more parametric effects, and hence the development of a more comprehensive, more accurate model.

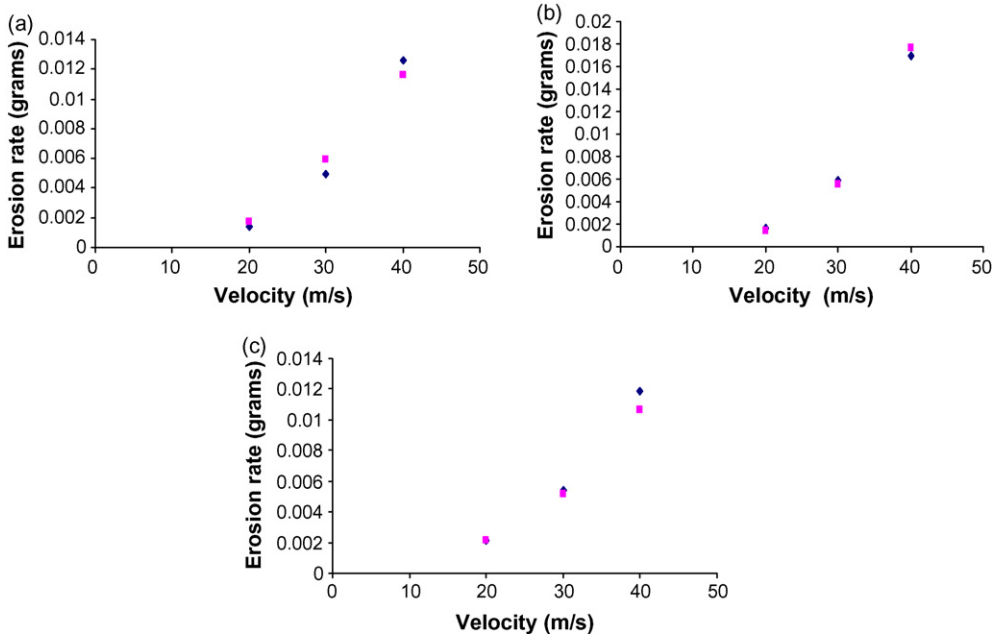

Fig. 11. (a) Erosion rate as a function of particle velocity with reference to Alumina-A target. (b) Erosion rate as a function of particle velocity with reference to Alumina-B target. (c) Erosion rate as a function of particle velocity with reference to Alumina-C target.

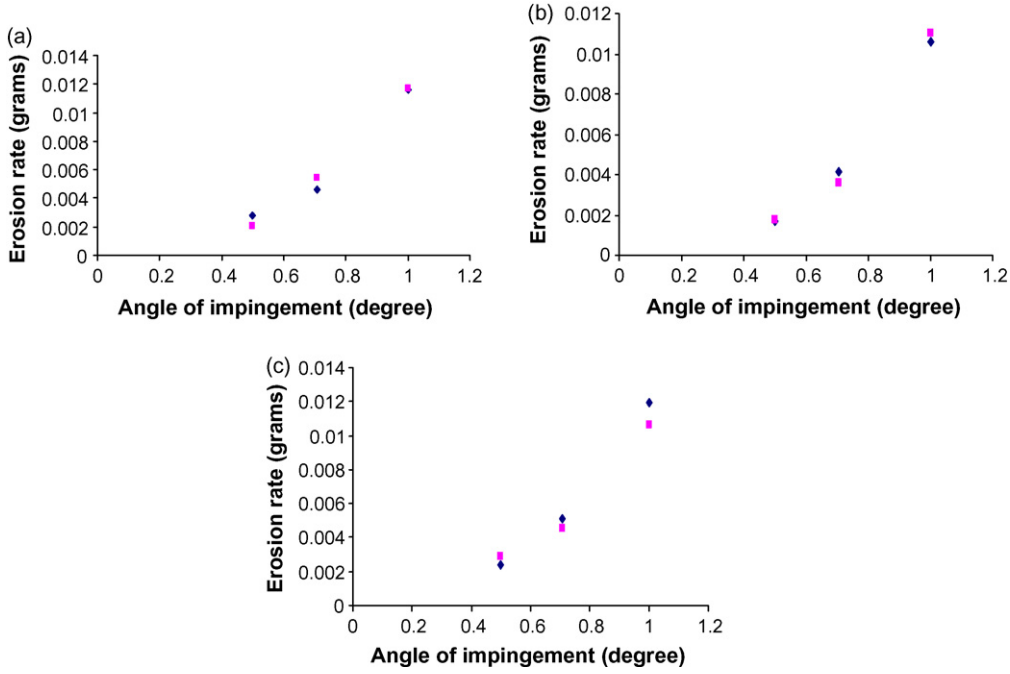

Fig. 12. (a) Erosion rate as a function of angle of impingement with reference to Alumina-A target. (b) Erosion rate as a function of angle of impingement with reference to impingement with reference to Alumina-B target. (c) Erosion rate as a function of angle of Alumina-C target.

Table 5
High level analyses for air-jet erosion

Parameter	Exponent/polynomial	
	Experimental predictions	Most-cited literature model
Velocity (m/s)	2.9	2.8
Angle of impingement (°)	2.3	2.0
Feed rate (g/m)	0.12	–
Particle hardness (GPa)	$0.0004P_H^2 - 0.014P_H + 0.13$	−0.25
Particle size (μm)	$-2 \times 10^{-5} d_p^2 + 0.004 d_p - 0.172$	0.66
Target density (g/cm^3)	$1.11\rho_t^2 - 8.0\rho_t + 14.50$	–
Particle density (g/cm^3)	$-0.0084\rho_p^2 + 0.05\rho_t - 0.052$	1.3
Target hardness (kg/mm^2)	$-3 \times 10^{-8} T_H^2 + 9 \times 10^{-5} T_H - 0.06$	–
Crack length (μm)	$6 \times 10^{-5} C_L^2 - 0.0054 C_L + 0.13$	–
Young's modulus (GPa)	$-5 \times 10^{-7} Y_M^2 + 0.0003 Y_M - 0.032$	–
Shear modulus (GPa)	$-4 \times 10^{-6} S_M^2 + 0.001 S_M - 0.035$	–

Table 6
High level analyses for slurry erosion

Parameter	Exponent/polynomial	
	Experimental predictions	Most-cited literature model
Flow rate (lpm)	5.14 (15–17.5), 0.85 (17.5–20)	−0.36
Angle of impingement (°)	1.5	1.6
Particle hardness (GPa)	3.5	–
Particle size (μm)	0.84	–
Particle concentration (10 g/l)	−0.31	−0.36
Target density (g/cm^3)	$5.08\rho_t^2 - 36.8\rho_t + 66.6$	–
Particle density (g/cm^3)	$-0.008\rho_P^2 + 0.05\rho_t - 0.05$	−0.36
Target hardness (kg/mm^2)	4.2	–
Crack length (μm)	$0.0005C_L^2 - 0.05C_L + 1.043$	–
Young's modulus (GPa)	$-3 \times 10^{-5} Y_M^2 + 0.0014 Y_M - 0.183$	–
Shear modulus (GPa)	$-2 \times 10^{-5} S_M^2 + 0.004 S_M - 0.2$	–

8. Conclusion

Experiments conducted to validate literature models have yielded several interesting results. Comparison was made between most-cited literature models and models formulated on the basics of current experiments. Slurry erosion results appear to be more in line with theoretical prediction than dry-impact erosion results, although both show good agreement. This may be due to the fact that particulate flow can be controlled much more easily in a slurry erosion tester. Refined models are proposed for air-jet and slurry-erosion on ceramics. Higher order effects can also be assessed from the available data, but with considerably less statistical significance due to fewer number of data points for analysis.

References

[1] P.H. Shipway, I.M. Hutchings, The role of particle properties in the erosion of brittle materials, Wear 193 (1996) 105–113.
[2] Hutchings, TRIBOLOGY: Friction and Wear of Engineering Materials, Edward Arnold, London, 1992, pp. 184–185.
[3] J. Zhou, S. Bahadur, The effect of material composition and operational variables on the erosion of alumina ceramics, Wear 150 (1991) 343–354.
[4] J.L. Routbort, R.O. Scattergood, A.P.L. Turner, The erosion of reaction-bonded SiC, Wear 59 (1980) 363–375.
[5] T.H. Kosel, Solid Particle Erosion, vol. 18, ASM International, 1992, pp. 199–211.
[6] J.L. Routbort, M.E. Gulden, Marshall, et al., Particle size distribution effects on the solid particle erosion of brittle materials, Wear 71 (1981) 363–373.
[7] R.O. Scattergood, J.L. Routbort, A.P.L. Turner, Velocity and size dependence of the erosion rates in silicon, Wear 67 (1981) 227–232.
[8] Z. Feng, A. Ball, The erosion of four materials using seven erodent—towards an understanding, Wear 233–235 (1999) 674–684.
[9] I. Finne, Some reflections on the past and future of erosion, Wear 186–187 (1995) 1–10.
[10] H.C. Meng, K.C. Ludema, Wear models and predictive equations: their form and content, Wear 181–183 (1995) 443–457.
[11] Y.I. Oka, H. Ohnogi, T. Honogi, T. Hosokawa, M. Matsumura, The impinging angle dependence of erosion damage caused by solid particle impact, Wear 203–204 (1997) 573–579.
[12] Y. Zhang, Y.-B. Cheng, S. Lathabai, Erosion of alumina ceramics by air- and water-suspended garnet particles, Wear 240 (2000) 40–51.
[13] J.E. Ritter, L. Rosenfeld, K. Jakus, Erosion and strength degradation in alumina, Wear 111 (1986) 335–346.
[14] E. Raask, Erosion Wear in Coal Utilization, Hemisphere Publishing Corporation, USA, 1988, pp. 22–23.
[15] D. Galuseket, P.C. Twigg, F.L. Riley, Wet erosion of liquid phase sintered alumina, Wear 233–235 (1999) 588–595.
[16] P.R. Marur, V.H. Tippur, Evaluation of mechanical properties of functionally graded materials, J. Test. Eval. 20 (1998) 539–549.
[17] I.M. Hutchings, Solid Particle Wear Testing, vol. 8, ASM International, 2000, pp. 343–344.
[18] V. Raghavan, Material Science and Engineering: A First Course, 4th ed., Prentice-Hall, India, 2001, pp. 232–233.